Optical and Quantum Electronics (2024) 56:63
https://doi.org/10.1007/s11082-023-05677-w

The impact of gallium ions on borosilicate glasses for structural, optical and biological applications

Taha M. Tiama[1] · A. Ibrahim[2,3] · M. Y. Hassaan[3] · Ahmed F. Mabied[4]

Received: 20 September 2023 / Accepted: 28 October 2023 / Published online: 2 December 2023

Abstract

This study demonstrates the significant impact of gallium ions on the local structure and physical, optical, and biological properties of borosilicate glasses. The glass composition, denoted as BSCZG, with the formula ($50B_2O_3$–$5SiO_2$–$15ZnO$–$(30\text{-}x)CaO$–xGa_2O_3), where $0 \leq x \leq 20$ mol%, was synthesized using the melt quenching technique. X-ray diffraction (XRD) patterns confirmed the amorphous nature of the BSCZG samples, presenting a broad hump. Analysis of the attenuated total reflectance Fourier-transform infrared spectroscopy (ATR-FTIR) results revealed the transformation of BO_4 units into BO_3 units, accompanied by generating non-bridging oxygens (NBOs) with increasing Ga_2O_3 content. As Ga_2O_3 content increased from 0 to 20 mol%, the experimental density (ρ_{exp}) and molar volume (V_m) of BSCZG glasses also increased, shifting from 2.70 to 3.14 g cm^{-3} and from 24.66 to 29.58 cm^3 mol^{-1}, respectively were also observed. This increment in V_m can be attributed to the rise in NBOs. Furthermore, an inverse relationship was observed between the optical band gap (E_{opt}) and optical band tail energy (E_U); *E*opt decreased from 3.27 to 3.08 eV, while E_U increased from 0.20 to 0.25 eV with the Ga_2O_3 content rising from 0 to 20 mol%. The refractive index (n) of BSCZG glasses also increased from 1.52 to 1.57 as Ga_2O_3 content increased. Additionally, XRD patterns and ATR-FTIR spectra of BSCZG confirmed the formation of hydroxyapatite (HA) following assessment in simulated body fluid (SBF) for 3, 7, and 14 days. Protein adsorption in phosphate-buffered saline (PBS), cell viability (MTT) assays using Vero cells, and immersion in SBF were conducted to assess the bioactivity of the prepared samples. The results indicated that gallium ions containing borosilicate glasses exhibited significantly higher degradation rates than the Ga-free glass sample. Despite increased chemical durability, the substituted glasses displayed a favorable in vitro bioactive response. SBF results suggested that BSCZG glasses were more likely to contain higher concentrations of HA due to the elevated content of Ga ions. In conclusion, borosilicate glasses incorporating Ga^{3+} ions demonstrate promising effects for both optical and biomedical applications.

Keywords Borosilicate glass · FTIR · Galliuim oxide · Biological activity · Optical band gap · Protein adsorption in phosphate-buffered saline (PBS) · Cell viability

Extended author information available on the last page of the article

1 Introduction

In recent years, there has been extensive research in the field of glass science, driven by the quest for advanced materials with multifunctional properties (Blanc et al. 2023). Glass, renowned for its exceptional versatility, has become the focal point of comprehensive research spanning various disciplines. This prominence is owed to the remarkable combination of inherent qualities of glass, including transparency, thermal resilience, mechanical robustness, and chemical inertness (Blanc et al. 2023; Lai et al. 2016). The ability to precisely tailor these properties to suit specific applications has led to the development of doped glasses. Doped glasses involve the introduction of distinct elements or compounds, resulting in significant alterations in the material's characteristics. Borosilicate glasses (BSGs) have attracted considerable attention from the scientific and engineering communities (Lai et al. 2016). These glasses represent a blend of desirable attributes found in both silicate and borate glasses, combining network-forming elements, namely borate and silicate (Mansour et al. 2021). This unique composition allows borosilicate glasses to harness the advantageous characteristics of borate glasses, such as their low melting points, thermal stability, and optical transparency (Lai et al. 2016; Mansour et al. 2021). Simultaneously, they benefit from the enhanced mechanical and chemical stability of silicate glasses (Tostanoski et al. 2022).

Borosilicate glasses have found widespread utilization across various applications, encompassing pharmaceutical vessel construction, bioactive glass formulations, optical instrument fabrication (Mansour et al. 2021), display screen production (Tostanoski et al. 2022), and the creation of colored ceramics suitable for low-temperature processes (Mansour et al. 2021). It has been recognized that zinc ions (Zn^{2+}), possessing a $3d^{10}$ electron configuration, do not exhibit probable $3d^{10}$–$3d^{10}$ electronic transitions (Sayyed et al. 2018). Consequently, the incorporation of ZnO into borate glasses results in colorless glass formations (Sayyed et al. 2018; El-Daly et al. 2021). In fact, ZnO plays a dual role in such glasses, functioning both as a glass former (comprising ZnO_4 structural units) and a glass modifier (comprising ZnO_6 structural units) (El-Daly et al. 2021). Additionally, introducing ZnO through doping can effectively lower the glass's melting temperature while preserving its other essential properties. Furthermore, the coordination of Zn^{2+} ions can be adjusted to tailor the glass structure according to specific requirements for precise applications (El-Daly et al. 2021).

Borosilicate glasses play a pivotal role in various applications across fields such as optics, electronics, biomedicine, and engineering. The influence of CaO as a network modifier significantly impacts different glass properties (Ibrahim et al. 2023a). However, tailoring properties to specific applications often requires the incorporation of dopants, including Ga_2O_3, Fe_2O_3, V_2O_5, or Gd_2O_3, which enable precise control of the material's characteristics (El-Daly et al. 2021; Ibrahim et al. 2023a, 2023b; Boyjoo et al. 2016; Al-Hadeethi et al. 2019).

Gd_2O_3, in particular, has garnered considerable attention as a versatile dopant capable of inducing substantial transformations in the glass structure, physical properties, optical behavior, and bioactivity (Al-Hadeethi et al. 2019). Similarly, Ga_2O_3 is renowned for its remarkable ability to adopt various coordination states, allowing it to bond with different glass network formers and thereby orchestrate modifications in glass structure and properties (Rana et al. 2017). Including Ga_2O_3 in B_2O_3–SiO_2–ZnO–CaO glasses holds promise for altering local atomic arrangements and coordination states (Rana et al. 2017). Consequently, these changes may lead to variations in glass density, thermal expansion

coefficients, and glass transition temperatures. These modifications in glass network connectivity and rigidity can, in turn, influence mechanical properties like hardness and fracture toughness (Boyjoo et al. 2016; Ibrahim et al. 2023b; Al-Hadeethi et al. 2019; Rana et al. 2017). Therefore, understanding these structural variations comprehensively becomes essential for fine-tuning these glasses for specific applications. Furthermore, deliberately doping B_2O_3–SiO_2–ZnO–CaO glasses with Ga_2O_3 can enhance various physical properties (Rana et al. 2017). This includes the modulation of electrical characteristics, such as conductivity and dielectric constants, making these glasses suitable for applications in electronics and sensing (El-Daly et al. 2021; Rana et al. 2017). The importance of optical properties in doped glasses cannot be overstated, especially in their relevance to photonics, optoelectronics, and telecommunications (Ballato and Dragic 2021). Including Ga_2O_3 in the glass matrix influences critical parameters, such as the optical bandgap, refractive index, and transparency range of B_2O_3–SiO_2–ZnO–CaO glasses. Fine-tuning these parameters through deliberate doping provides a pathway to optimize these glasses for specific optical applications, whether UV filtration, laser emission, or waveguide functionalities (Ibrahim et al. 2023a; Al-Hadeethi et al. 2019; Ballato and Dragic 2021).

The bioactive materials that known as bioactive glasses (BGs), first created by Hench in 1969 (45S5), are considered to suggest attractive bioactivity and biocompatibility; Na_2O, CaO, P_2O_5, and SiO_2 system is the basis for the majority of them (Jones 2013). Bioactive glasses can be broadly categorized into three classes based on the representative former oxide present in the formulation, namely SiO_2-based (silicate), B_2O_3-based (borate), and P_2O_5-based (phosphate) systems. Borate glasses have stronger reactivity than silicate glasses, which lead to faster bioactive kinetics (Brink et al. 1997). Other oxides may be added to its chemical composition to provide glass with particular uses (Tiama et al. 2023). Bioactive glasses have received the greatest attention in bone regeneration research due to their enticing bioactive qualities and their potential to bind with bone (Tripathi et al. 2016). So, these glasses promote bone and cell growth, and the immersion of bioactive glasses within the body produces a hydroxyapatite (HA) layer that links hard tissues and soft tissues (Kamal and Hezma 2018). In a mouse model, using bioactive borate glass coated with hydroxyapatite HCA nanoparticles was successful in wound healing (Chen et al. 2021). Previous research showed that as boron concentration increased, the precipitated hydroxyapatite (HA) increased, implying that the biological behavior substantially improved due to the integration of boron in bio-glass synthesis (Kamal and Hezma 2018; Chen et al. 2021). Furthermore, at a lower extracted dosage, B_2O_3 supplementation has favored the cell proliferation of human periodontal ligament cells (HPDLCs) (Bai et al. 2021; Ren et al. 2018).

On the other hand, borosilicate glass has been found to aid tissue infiltration, cell proliferation, and differentiation in vitro (Vallet-Regí et al. 2017). BGs are a unique biomaterial used for many biological applications, including bone regeneration, wound healing, and other medical applications such as cancer treatment (Jones 2013; Hench et al. 2014). Also, BGs have a high capacity for mineralization, good bone conductors, osteoclasts, and conductors, and they form strong interfacial bonds with soft and hard tissues (Ojansivu et al. 2018; Vallet-Regi et al. 2001). The borosilicate vitreous positively affected the adhesion of the HASC skeletal system. In many osteogenic indicators studied, borosilicate glass outperforms others in cell culture (Vallet-Regi et al. 2001; Doadrio et al. 2017). Depending on their composition, BGs may improve vascularization, wound healing, anti-inflammatory reactions, as well as bacterial growth (Zheng and Boccaccini 2017).

Additional therapeutic ions, such as Cu, Zn, Mg, Ag, Ga, and Ce, can be introduced into the silica network to offer specific biological activities to BGs (e.g., osteogenesis,

angiogenesis, anti-inflammatory response, antibacterial activity) (Zhu et al. 2021). BGs can be modified to transport pharmaceuticals (antibiotics, enzymes, growth factors) and physiologically active ions for particular biomedical applications (Zheng and Boccaccini 2017; Zhu et al. 2021).

In contrast, inorganic materials have been widely used in tissue regeneration. The importance of adding therapeutic metal ions to BG for bone formation and angiogenesis was recognized in previous studies (Zheng and Boccaccini 2017; Zhu et al. 2021; Assis et al. 2022). Previous studies showed that gallium (Ga) ions improved the treatment of bone absorption, osteoporosis, and hypercalcemia associated with cancer (Zhu et al. 2021; Deliormanlı 2015). It also inhibits osteoporotic bone resorption without damaging osteoblasts (Collery et al. 2002). Also, it was the second metal ion that used in cancer treatment after platinum (Franchini et al. 2012). In metabolic bone, cancer, and infectious diseases, some gallium compounds might be employed as diagnostic and therapeutic techniques (Wren et al. 2013). It is a drug that has already received clinical approval and that showed abilities to lower blood calcium levels and prevent bacterial activity (Wren et al. 2013; Valappil et al. 2009). It is also crucial for recognizing the crystalline phases that precipitate in the glass materials (Mabied et al. 2022).

In this work, novel borosilicate glasses doped by Ga_2O_3 have been prepared. Furthermore, this study aims to investigate the effect of gallium ions on the local structure physical, optical, and bioactive properties of borosilicate glasses networks using XRD, experimental density, FTIR and UV–Vis-NIR, protein adsorption, and cell viability. In addition, we aim to understand the characteristics of Ga^{3+} doped borosilicate-based glasses for biomedical applications. Furthermore, the effect of Ga^{3+} upon the in vitro bioactivity of protein adsorption will be evaluated using Phosphate Buffered Saline (PBS) under static conditions, and the cell viability of all compounds (MTT) using Vero cells and a simulated body fluid (SBF) experiment will be assessed.

2 Experimental methods

2.1 Samples preparation

Borosilicate-based glasses, denoted as BSCZG, were synthesized using the melt-quenching method. The composition of these glasses was [$50B_2O_3$–$5SiO_2$–15ZnO–(30-x)CaO–xGa_2O_3] where x ranged from 0 to 20 mol%. High-purity raw chemical materials, including B_2O_3, SiO_2, ZnO, $CaCO_3$, and Ga_2O_3, were meticulously weighed in the required mol% ratios and mixed well in a ceramic mortar. The resulting mixture was placed in a platinum crucible and melted at 1300 °C in an electric furnace for 2 h. Afterward, the molten BSCZG of each sample was cast between the copper disks at room temperature. The BSCZG glasses underwent a heat treatment process at 350 °C for 5 h to alleviate internal thermal stress. These procedures yielded transparent glass samples with a faint yellowish hue. The entire process of preparing the glass samples is visually summarized in Fig. 1.

2.2 Characterization

X-ray diffraction patterns (XRD) of the BSCZG glasses, both as-prepared and after immersion in simulated body fluid (SBF), were acquired using a modern Bruker d8 advance

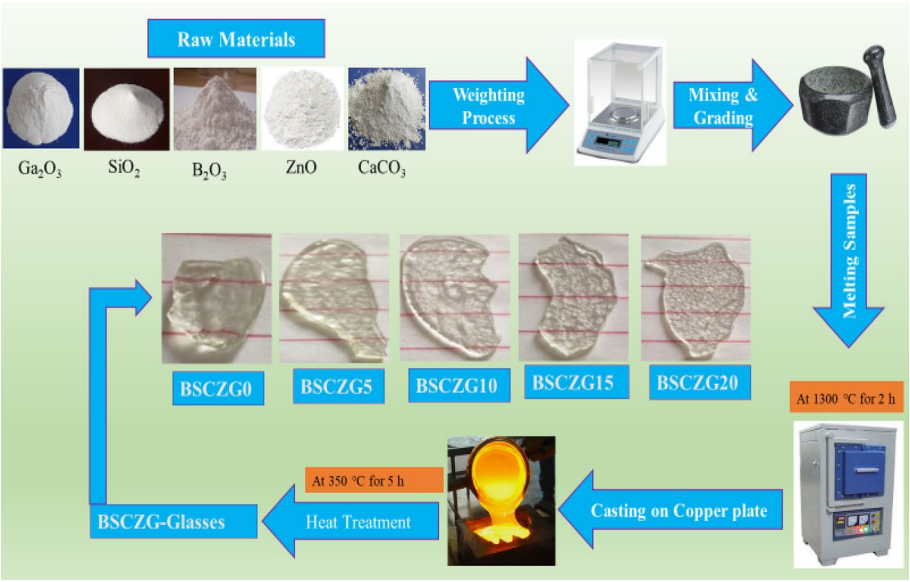

Fig. 1 The schematic diagram illustrates the methods used to obtain the BSCZG glasses in practice

diffractometer. The measurements were conducted with a Cu-Kα source (wavelength, λ = 1.542 Å), at 300 mA and 40 kV, covering a 2θ range from 5° to 80°.

Fourier Transform Infrared spectroscopy (FTIR) absorption spectra of the BSCZG glasses for the as-prepared samples and after immersion in SBF were recorded using a Bruker Vertex 70 spectrometer from Germany. The spectral resolution was set at 4 cm^{-1}, and the wavenumber range was between 400 and 4000 cm^{-1}.

The experimental density (ρ_{exp}) of the BSCZG glasses was determined using the Archimedes method with carbon tetrachloride (CCl_4) as the immersion liquid, which has a known density of $\rho_l = 1.592$ g cm^{-3}. The molar volume (V_m) was calculated based on the ρ_{exp} values and molar mass (M_w), with detailed procedures outlined in Sect. 3.3 of the results and discussions.

For optical measurements, polished glass plates with a surface area of about 1.5 cm^2 and a thickness of about 1.5 mm were used for transmittance and absorbance spectroscopy. Prior to measurements, the BSCZG glasses underwent polishing using 80 and 180 grits. Optical absorption spectra were recorded using an Agilent Technologies Cary 5000 UV–Vis-NIR spectrophotometer in the wavelength range of 190–2500 nm, with a resolution of 2 nm.

2.3 Protein adsorption

The protein adsorption ability was investigated on sample surfaces as part of the physiological behavior research for the produced samples. Bovine serum albumin (BSA) was chosen as the representative protein for this study. Under controlled conditions of pH = 7.4 and a temperature of 37 °C, 0.2 g of BSA was introduced into 200 ml of phosphate-buffered saline (PBS). Within this solution, an additional 0.4 g of each sample (in powder form) was

added to a 40-ml aliquot. The adsorption process was carried out for 1 h at 37 °C within an incubator. Following the adsorption period, the samples underwent a thorough washing procedure involving three rinsing cycles with PBS and distilled water. This process aimed to eliminate any unattached proteins and salt residues. Subsequently, the samples were dried at 37 °C. The FTIR technique was utilized to assess the capacity of proteins to bind to the surfaces of the samples.

2.4 Cell viability

The evaluation of cell viability for each drug was conducted through a 3-(4,5 dimethylthiazol-2-yl)-2,5-diphenyltetrazolium bromide (MTT) experiment using Vero cells. This assay relies on the reduction of tetrazolium salts into soluble formazan crystals, which are spectrophotometrically measurable. Initially, cells were seeded in a 96-well plate at 104 cells per well density and incubated overnight at 37 °C with 5% CO_2. The following day, cells were individually treated with sequential doses of each chemical. After 48 h of incubation, 30 µl of a 5 mg/mL MTT solution was added to each well and incubated at 37 °C for 3 h. Subsequently, the cell culture medium was carefully aspirated, and 200 µl of dimethyl sulfoxide was added to each well to dissolve the insoluble formazan crystals. The absorbance at 570 nm was measured using a multimode microplate reader (CLARIO star Plus, BMG LABTECH, Germany). The CC_{50} (cytotoxic concentration at which 50% of cells are affected) was calculated using GraphPad Prism software through non-linear regression analysis with the log(inhibitor) versus normalized response-variable slope model.

2.5 Simulated body fluid

The samples were immersed in a simulated body fluid (SBF) solution at around 37 °C for one to fourteen days. According to Kokubo and Takadama (Quintero Sierra and Escobar 2019), SBF is produced by dissolving a mixture of salts, including NaCl, $NaHCO_3$, KCl, $K_2HPO_4.3H_2O$, $MgCl_{2\cdot 6}H_2O$, and Na_2SO_4, in distilled water and then buffering the mix with a tris and HCl solution to obtain a pH of 7.4. All of the chemicals were obtained from Sigma Aldrich.

3 Results and discussions

3.1 XRD

XRD patterns of BSCZG0 and BSCZG20 as-prepared samples showed a broad hump, confirming the amorphous nature of the prepared glass samples, as shown in Fig. 2.

3.2 FTIR spectroscopy of as-prepared glass samples

FTIR is one of the most essential non-destructive techniques used in several science fields for studying the structure of the samples. It determines the functional groups of materials, such as glass samples (Catauro et al. 2015). Zhou et al. (Vukajlovic et al. 2021) informed that borosilicate glasses include boroxol rings like (B_3O_6) connected by the BO_3 units. The present study focuses on the relation between BO_3 and BO_4 units and NBOs as a function

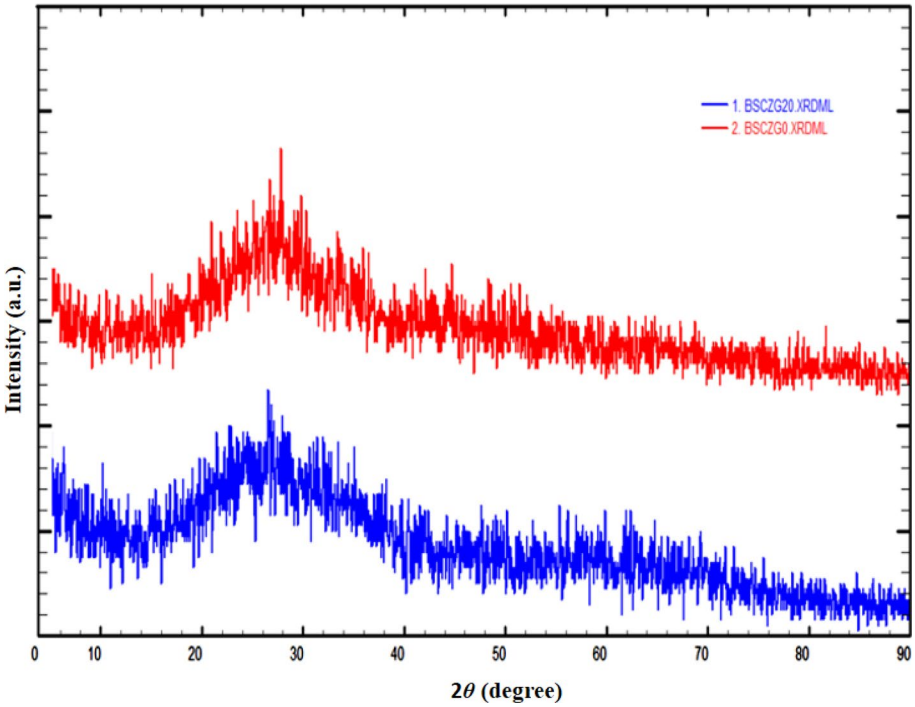

Fig. 2 XRD profiles of powder BSCZG0 and BSCZG20-glasses

of Ga_2O_3 content. Information about the formation of non-bridging oxygen NBOs by the transformation between BO_4 and BO_3 units can be obtained. Once glass modifiers (such as CaO) are introduced into borosilicate glass, the conversion of BO_4 to BO_3 causes the formation of (NBOs) (Vukajlovic et al. 2021). Figure 3a shows that five spectral regions that characterize the FTIR absorption spectra of BSCZG. The absorption band within region V was observed between (1800–1600 cm^{-1}) this may be attributed to the hydroxyl group (OH^-) (Vukajlovic et al. 2021; Ibrahim et al. 2023c). The vibration bands in region IV are between 1600 and 1228 cm^{-1}, related to BO_3 units (Catauro et al. 2015; Vukajlovic et al. 2021). Region III represents the distinctive vibrations of BO_4 units (Vukajlovic et al. 2021) that observed at (1228–800 cm^{-1}). Region II refers to the configuration of bending modes in BO_3 units in the wavenumber range (800–600) cm^{-1}, which contains the B-O-B bending modes (Ibrahim et al. 2022). In region I, the absorption bands that observed in the wavenumber range of (600–400 cm^{-1}) are related to the vibrations of metal cations such as Ca^{2+}, Zn^{2+}, and Si–O–Si (Wren et al. 2013; Ibrahim et al. 2022). Depending on the change in the composition of the BSCZG, these five zones shifted to higher wavenumbers, as Ga_2O_3 content was increased. It combines superposition and smaller absorption bands that are contained in wide band. These broad bands may be divided into small bands, each small band belonging to a specific structural group. The deconvolution of these spectra using Origin software's "many peaks fit" method, to extract the five areas into discrete bands, as shown in Fig. 3a.

Table 1 lists the peak positions (x_c) and the assignments for each peak obtained by the deconvolution process. Furthermore, a detailed recognition of the deconvoluted

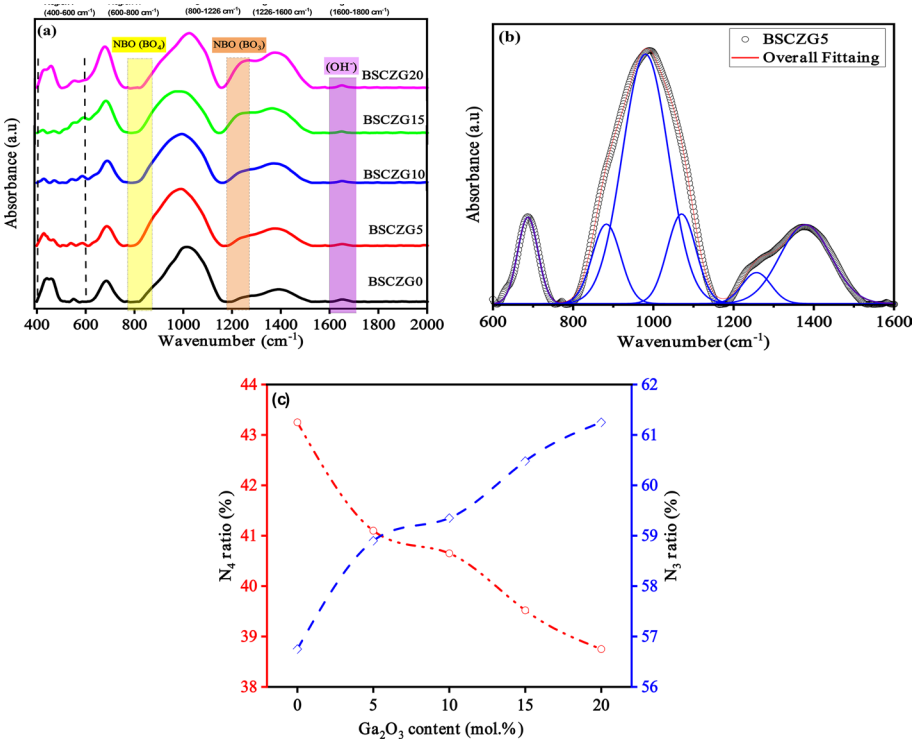

Fig. 3 **a** FTIR spectra of BSCZG glasses with '*x*' of 0, 5,10, 15, and 20 mol% Ga_2O_3 content, **b** Deconvoluted infrared bands of the sample doped with Ga_2O_3 = 5 mol%, **c** Variation of the N_4 and N_3 of BSCZG-glass

bands leads to the following assignments about the structural changes that caused by increasing Ga_2O_3 content. The small absorption peak at 422 cm^{-1} may be ascribed to Ca–O vibrations (Collery et al. 2002; Catauro et al. 2015). According to Fig. 3a and Table 1, the peak shifted to a lower wavenumber, and its intensity decreased with decreasing CaO content from 30 to 10 mol%. The absorption peak at 462 cm^{-1} is due to Si–O–Si bending vibration in SiO_4 tetrahedra (Vukajlovic et al. 2021; Ibrahim et al. 2022; Zhou et al. 2021). This peak shifted slightly toward a smaller wavenumber as Ga_2O_3 content was increased and its intensity decreased from BSCZG0 to BSCZG15, while it increased at BSCZG20. Due to the in-plane bending of the BO_3 unit (Ibrahim et al. 2022), a small peak at 585 cm^{-1} appeared as Ga_2O_3 was increased. This peak is ascribed to the asymmetric vibration of Si–O–Si (Zhou et al. 2021).

The strong absorption peak at 684 cm^{-1} is allocated to B–O–B bending vibration in symmetric BO_3 triangles (Catauro et al. 2015; Vukajlovic et al. 2021; Ibrahim et al. 2023c, 2022). Moreover, Fig. 3a shows that the intensity of this peak increased gradually with increasing Ga_2O_3 content. Additionally, a significant peak in this study was observed in Fig. 3b at 886 cm^{-1}, which is ascribed to the stretching of BO_4 units and starching vibration of non-bridging oxygens (NBOs) of BO_4 groups as well as Si–O–Si symmetric vibrations (Catauro et al. 2015; Ibrahim et al. 2022). According to the deconvolution data, the area under this peak decreased gradually with increasing Ga_2O_3 content, which means that

Table 1 Band assignment for FTIR spectra of BSCZG -glasses

No. peak	Sample					
	Band center (cm^{-1})					Peak assignments
	BSCZG0	BSCZG5	BSCZG10	BSCZG15	BSCZG20	
1	438	428	425	421	422	Cai–O and Zn–O vibration
2	462	467	472	467	460	Si–O–Si bending vibration in SiO_4 tetrahedral
3	544	542	539	534	542	Asymmetric vibration of Si–O–Si
4	–	585	587	586	–	Deformation of the BO_3 unit
5	684	687	690	682	681	B–O–B bending vibration in symmetric BO_3 triangles
6	886	882	889	868	894	Associated with Si–O–Si symmetric vibrations as well as stretching of BO_4 units and starching vibration of non-bridging oxygens (NBOs) of BO_4 groups
7	981	980	989	974	981	Vibrations of B–O bonds in BO_4unit
8	1002	–	995	998	1024	Stretching vibrations of B–O bonds in BO_4 units
9	1091	1070	1083	1074	1108	Penta-borate units
10	1241	1239	1256	1269	1265	B–O vibrations of non-bridging oxygens (NBOs) in the BO_3 units
11	1388	1386	1388	1367	1379	B–O vibrations of bridging oxygens within the BO_3 units
12	1656	1655	1653	1651	1656	Hydroxyl group $(OH)^-$

the amount of NBOs in BO_4 decreased. A peak at 981 cm^{-1} is ascribed to the vibration of B-O bonds in the BO_4 unit (Catauro et al. 2015). A strong absorption peak observed at around 1002 cm^{-1} is attributed to bending vibrations of B-O bonds in BO_4 units from tri-, tetra-, and Penta-borate groups (Vukajlovic et al. 2021; Ibrahim et al. 2022). The center of the peak shifted to a higher wavenumber from 1002 to 1024 cm^{-1} with the increasing content of Ga_2O_3 from 0 to 20 mol%. The absorption peak observed at 1091 cm^{-1} may be ascribed to penta-borate units (Catauro et al. 2015; Vukajlovic et al. 2021). The center of the peak shifted to a higher wavenumber with increasing Ga_2O_3 content. Hence, the absorption peak located in the range (1241–1265 cm^{-1}) is essential for understanding the variation in the structure of the glass matrix. Based on the data, this peak is related to the B-O vibrations of non-bridging oxygens (NBOs) in the BO_3 units (Catauro et al. 2015; Vukajlovic et al. 2021; Ibrahim et al. 2023c, 2022), and its intensity increases with increasing Ga_2O_3 content. Additionally, the data obtained after the band disintegration showed that the area under peak increased with the increasing Ga_2O_3 content, this is reflected in the possibility of producing NBOs markedly. A strong absorption peak at 1338 cm^{-1} is attributed to the B-O vibrations of bridging oxygens within the BO_3 units (Vukajlovic et al. 2021; Ibrahim et al. 2022). The center of the peak was shifted to a lower wavenumber by adding Ga ions to the glass matrix from 1388 to 1379 cm^{-1}, as shown in Table 1. Also, the peak intensity was increased with the increasing Ga_2O_3 content from 0 to 20 mol.

On the other hand, based on the results summarized in Table 1 and shown in Fig. 3b, one can calculate N_4 using the following equation (Vukajlovic et al. 2021; Ibrahim et al. 2022). During N_4 calculations, we did not consider the relative areas of individual bands less than 886 cm^{-1}.

$$N_4 = \frac{A(BO_4)}{A(BO_4) + A(BO_3)} \tag{1}$$

where $A(BO_4)$ is the total area under the absorption peaks at (1228–800 cm^{-1}) and $A(BO_3)$ is the total area under the absorption peaks at (1600–1228 cm^{-1} and 800–600 cm^{-1}).

From Fig. 3c, we notice the linear decrease in N_4 from 43.25 to 38.75% with the increase of the Ga_2O_3 content. As a result, the continuous replacement of Ga_2O_3 by CaO causes a decrease in the N_4 ratio (as shown in Fig. 3c) and, as a result, a steady increase in NBOs in the glass matrix could be observed. The significant drop in the N_4 ratio with increasing Ga_2O_3 concentration means that BO_4 groups decrease and BO_3 units increase causing the generation of NBOs in the glass matrix.

3.3 Physical properties

Density is one of the simple and easy method by which we know some information about changes in a material due to changing chemical composition. As it is a macroscopic method, it is probable to identify the structural variations in the glass network. Figure 4 shows the increase in experimental density (ρ_{exp}) and the molar volume (V_m) with the increase of Ga_2O_3 content.

A gradual increase in both (ρ_{exp}) and (V_m) from 2.70 to 3.14 g cm^{-3} and from 24.66 to 29.58 cm^3 mol^{-1}, respectively, with the increase of the Ga_2O_3 content. The approximate increase in the (ρ_{exp}) of the sample that is free of Ga_2O_3 is 10, 12, 14, and 16% for BSCZG5, BSCZG10, BSCZG15, and BSCZG20 glasses, respectively. Since Ga_2O_3 has a greater molar mass than CaO (187.44 g. mol^{-1} vs. 56.07 g mol^{-1}), it was found that the

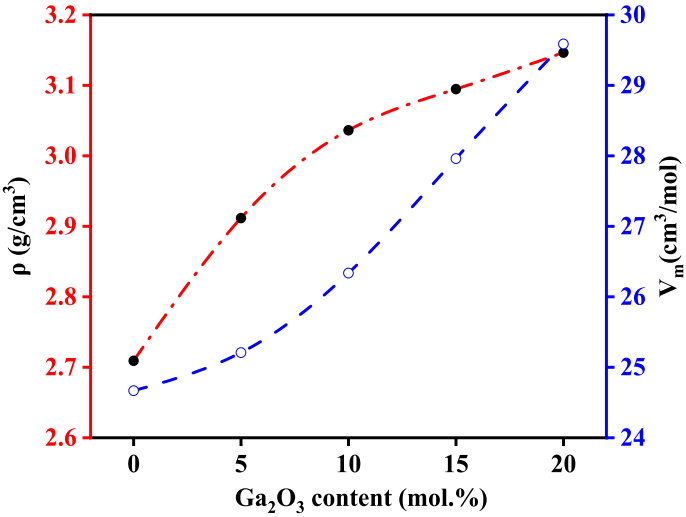

Fig. 4 Variation of the experimental density (ρ_{exp}) and molar volume (Vm) as a function of Ga_2O_3 content for all BSCZG -glasses

density increases as the amount of Ga_2O_3 in the glass matrix was increased. As a result, the significant increase in density can be attributed to this reason (Doadrio et al. 2017; Collery et al. 2002). Also, the values of (V_m) were increased with the replacement of CaO with Ga_2O_3 in the glass network (Collery et al. 2002). The approximate increase in the (V_m) of the BSCZG0 glass sample is 2, 7, 13, and 20% for BSCZG5, BSCZG10, BSCZG15, and BSCZG20 glasses, respectively. The increase in molar volume is likely due to the following possibilities: (1) Ga_2O_3 replaced CaO, which had one oxygen ion, with three oxygen ions, increasing the number of oxygen ions in the glass network. (2) According to the previously presented FTIR results, we can correlate the gradual increase of V_m for BSCZG-glasses with the increase in NBOs (alteration of BO_4 to BO_3 group), causing the formation of a glassy network that tends to be open structure (Vukajlovic et al. 2021). Therefore, based on (1) and (2) the increase in the V_m of BSCZG-glasses with Ga_2O_3 content. Furthermore, the ions (N) concentrations are calculated from the V_m via the formula in Table 2. It decreased from 2.44×10^{22} to 2.03×10^{22} (cm^{-3}), proportional to the increase of Ga_2O_3 content in the glass network. Also, this decrease can be ascribed to the increase in (V_m) values, as shown in Table. 2. Additionally, the interatomic distance values (r_i) are computed using the formula in Table 2. The r_i values were increased from 4.26 (Å) to 5.11 (Å) with more increase of Ga_2O_3 content from 0 to 20 mol%. This may represent the glass network's tendency to the open structure. Based on the calculated result of V_m and r_i are in good agreement with the results obtained by FTIR, whereas the increase in Ga_2O_3 content caused the increase in NBOs. In addition, the optical basicity (Λ_{th}) denotes the capability of oxide glasses to transport negative charges from the glass network to the probe ions (Ibrahim et al. 2023c, 2022; Zhou et al. 2021; Farouk et al. 2020). An oxide glass' acidic-base nature is determined by its electronegativity, using the equation in Table 2 (Abd El-Fattah et al. 2017). To begin, we multiply the (mol%) of oxide i (x_i) through its electronegativity (χ_i) and add them together to get the electronegativity of each mixture. The average electronegativity (χ_{avg}) acquired the optical basicity through replacement in the equation provided in Table 2. The electronic polarizability (α_0^{-2}) of oxide was a feature that lends to

Table 2 Some physical properties of BSCZG -glasses

Sample code	BSCZG0	BSCZG5	BSCZG10	BSCZG15	BSCZG20	Formula
Molar mass(M) (g/mol)	66.82	73.39	79.96	86.53	93.09	$M=\sum_i X_i m_i$
Density Experimental (ρ_{exp}) (g/cm^3) $\pm_{0.01}$	2.70	2.97	3.03	3.093	3.14	$\rho_{exp}=\frac{Wa}{Wa-Wl}l$
Density Empirical (ρ_{emp}) (g/cm^3)	3.20	3.36	3.51	3.67	3.82	$\rho_{emp}=\sum_i X_i m_i$
Molar volume (V_m)	24.66	25.20	26.33	27.96	29.58	$V_{exp}=\frac{Mw}{\exp}$
Concentration of ions (N)*10^{22} (cm^{-3}) $\pm_{0.01}$	2.44	2.38	2.28	2.15	2.03	$N_i=\frac{NA}{Vm}$
Interatomic separation, (r_i)	4.26	4.35	4.56	4.83	5.11	$r_i=\left(\frac{1}{N_i}\right)^{\frac{1}{3}}$
Interatomic separation in the glass matrix	1.37	1.40	1.46	1.55	1.64	$d_{B\text{-}B}=\left(\frac{Vm}{NA}\right)^{\frac{1}{3}}$
Average electronegativity (χ_{avg})	2.63	2.52	2.41	2.30	2.19	$\chi_{avg}=\sum_i x_i\chi_i$
Optical basicity (Λ_{th})	0.58	0.63	0.70	0.78	0.89	$\Lambda_{th}=\frac{0.75}{Xavg-1.35}$
Polarizability (α_0^{-2})	1.53	1.62	1.73	1.89	2.14	$\alpha_0^{-2}=\frac{1.67}{1.67-\Lambda th}$

x_i and i are the molar percent and density of oxide i. N_A is Avogadro's number. W_a and W_l are the weight of glass samples in the air and liquid respectively

the electronic and optical applications of the materials (Farouk et al. 2020; Abd El-Fattah et al. 2017). The computed values of (α_0^{-2}) are known by the empirical method; Table 2. It was observed that the values of α_0^{-2} and (Λ_{th}) increased as a function of increasing Ga_2O_3 content. According to Zhou et al. (2021); Abd El-Fattah et al. 2017), as the single bond strength decreases, which is lower for Ga_2O_3 (285 kJ mol^{-1}) than for CaO (464 kJ mol^{-1}), the values of optical basicity may be increased (Farouk et al. 2020; Abd El-Fattah et al. 2017; Ibrahim and Sadeq 2021).

The average values of α_0^{-2} and Λ_{th} for BSCZG glasses show a slight increase with increasing Ga_2O_3/CaO ratio, as the basic oxide of both CaO and Ga_2O_3 are close together, since ($\Lambda(n_o)=1.00$ for CaO) and ($\Lambda(n_o)=0.71$ for Ga_2O_3) (Abd El-Fattah et al. 2017). The minor increase in Λ_{th} and α_0^{-2} of the BSCZG glasses with increased Ga_2O_3 concentration might indicate an increase in electron localization and, as a result, an increase in localized donor pressure of the BSCZG-glasses network (Catauro et al. 2015; Abd El-Fattah et al. 2017).

3.4 Optical properties

The transmission spectra of BSCZG glasses in the UV, visible, and NIR ranges are shown in Fig. 5. Transmission results show that the BSCZG0 glass, which is free of Ga_2O_3, exhibits transmittance in the 400–1200 nm range. This range is typical of the visible and near-infrared spectra, roughly 53% at 1200 nm, indicating a reduced transparency degree for the BSCZG glasses. Meanwhile, after adding Ga_2O_3 to the glass matrix, the transparency of BSCZG glasses increases. As a result, the values of transparency were increased to 72% at the BSCZG20 glass. It is known that there are no

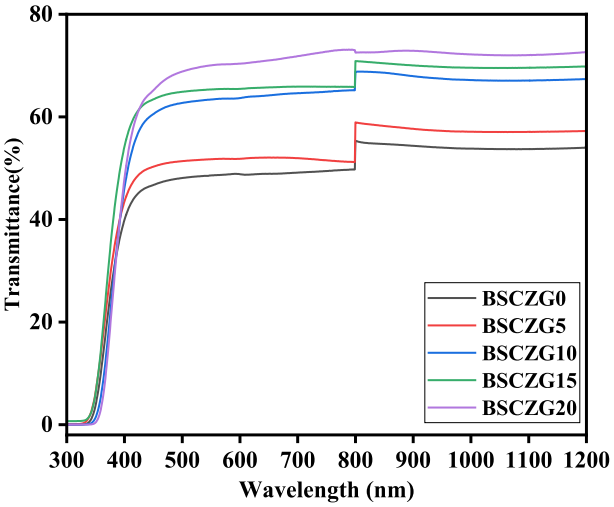

Fig. 5 UV–Visible-NIR optical transmittance versus wavelength for BSCZG- glasses

transmission peaks in infrared and visible absorption spectra in borosilicate glasses, this is one of their most distinguishing features (Ibrahim and Sadeq 2021).

The transition between the valance and conduction bands, *i.e.*, the energy gap, causes the absorption edge, or cut-off, in the near UV range. The absorption edge wavelength shifts towards the redshift as the Ga_2O_3 content in the BSCZG glasses increases.

The absorption coefficient (α) can be computed by the equation (Valappil et al. 2009):

$$\alpha(\upsilon) = \frac{1}{t} \log \frac{I_o}{I} \tag{2}$$

where $\frac{Io}{I}$ corresponds to the absorbance near the edge, and t is the thickness of the glass sample.

By the Mott-Davis relation, the optical band gap can be calculated based on absorption coefficients (Sistla and Seshasayee 2004):

$$\alpha(\upsilon) = B\frac{(h\upsilon - E_{opt})^z}{h\upsilon} \tag{3}$$

There are potential values of (z) that can be equal to 2, 1/2, 3, and 3/2, respectively, for indirect allowed, directly allowed, and indirectly forbidden transitions. The energy and momentum of an electron in an optical transition are retained equally in crystalline semiconductors, whereas only the energy is conserved in amorphous materials. The absorption of photons around E_{opt} in indirect band gap semiconductors, such as specific glasses, necessitates phonons' absorption and/or emission during absorption. The value for (z) in our glassy system is equal to 2, corresponding to the indirect transition (Zhou et al. 2021; Abd El-Fattah et al. 2017).

The values of E_{opt} are calculated by extrapolating the linear part of the spectrum, when $(\alpha h\upsilon)^{0.5}$ is plotted against photon energy (h υ) in (Fig. 6a–c). In Fig. 6d the values of E_{opt} are presented with increasing Ga_2O_3 concentration in BSCZG-glasses, and E_{opt} values rapidly decreased from 3.27 eV to 3.08 with increasing Ga_2O_3 from 0 to 20 mol%. A decrease in E_{opt} values is explained by an increase in NBOs in BBSCZG glasses with

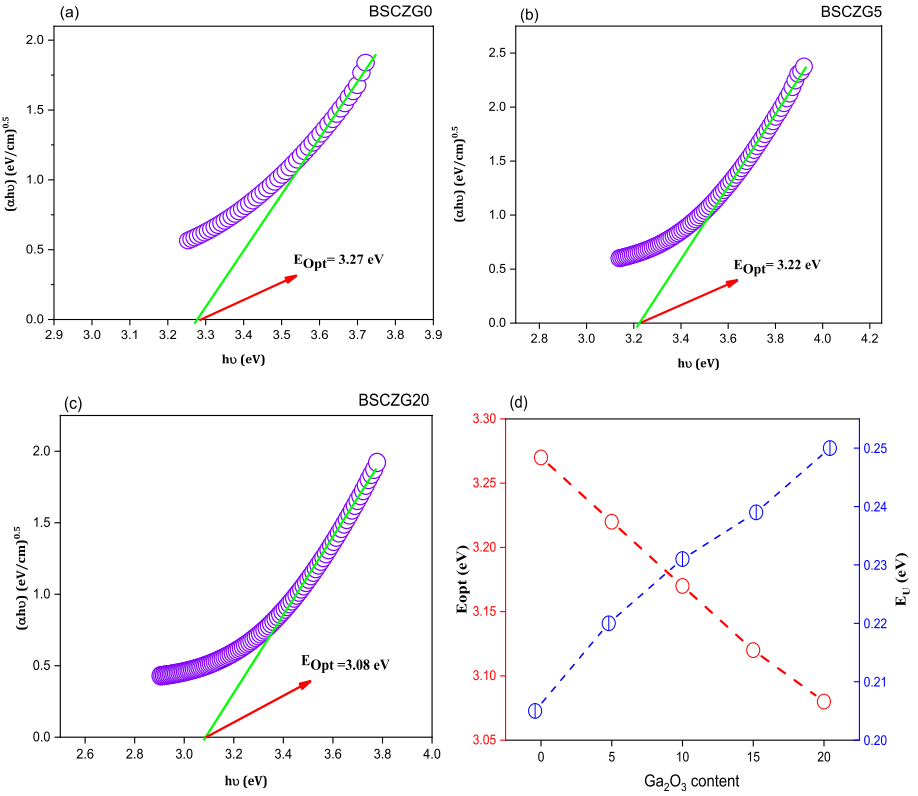

Fig. 6 The optical band gap of **a** BSCZG0, **b** BSCZG5, **c** BSCZG20, and **d** the variation of the optical band gap (E_{Opt}) and the optical band tail (E_U) for BSCZG-glass samples

the increasing Ga_2O_3 content. Moreover, increasing values of α_0^{-2} and $\wedge_{th}$ with increasing Ga_2O_3 additions can promote such a decrease in E_{opt} values. Furthermore, it was found that the obtained E_{opt} values were within the range of semiconductors.

The band tail width of absorption spectra can potentially reveal information regarding a probable variation in the glassy matrix (Ibrahim and Sadeq 2021). E_U is linked to $\alpha(\upsilon)$ by an exponential relationship for lower values of the absorption coefficient band tail (Ibrahim and Sadeq 2021; Sayyed et al. 2022):

$$\alpha(\upsilon) = \alpha_0 \exp\left(\frac{h\upsilon}{E_U}\right) \tag{4}$$

where E_U is the Urbach energy, α is a constant, and hυ is the photon energy. The width of the band tail of the localized states in the band gap is reflected by the Urbach energy. By plotting a relationship between lnα and hυ the value of E_U can be determined by the slope in the above relationship. A summary of the calculated values is provided in Table 3. The values of E_U increase from 0.20 to 0.25 eV with increasing Ga_2O_3 content from 0 to 20 mol%., as shown in Fig. 6d. These results are in good agreement with the results obtained from the FTIR part, where the results showed an increase in NBOs, increasing the

Table 3 Optical band gap (E_{Opt}), optical band tail (E_U), refractive index(n), and dielectric constant (ε_o) of BSCZG-glasses

Sample	Optical band gap (E_{Opt}) (eV)	Optical band tail (E_U) (eV)	Refractive index (n)	Optical dielectric constant (ε_o)
BSCZG0	3.27	0.205	1.52	2.32
BSCZG5	3.22	0.220	1.54	2.39
BSCZG10	3.17	0.231	1.56	2.44
BSCZG15	3.12	0.239	1.56	2.46
BSCZG20	3.08	0.25	1.57	2.48

localized state developed by the Ga_2O_3 amounts. Therefore, it is evident that gallium's ions addition make these glass samples a promising material for optoelectronic applications.

The refractive index (n) is particularly essential for optical glasses applications. The energy band gap and the density of oxide glasses are connected to the linearity of the refractive index, and n may be computed using the equation (Sayyed et al. 2022).

$$n_r = \frac{\rho_{\exp+10.4}}{8.6} \tag{5}$$

The refractive index ($\varepsilon_o = n^2$) (Sadeq and Ibrahim 2021) may be used to compute the optical dielectric constant. As a result, the Penn model can be stated as a function of the refractive index. The refractive index and optical dielectric constant of the BSCZG glasses vary with Ga_2O_3 content, as shown in Table 3. The refractive index (n) increased linearly from 1.52 for Ga-free glass to be 1.57 for high Ga_2O_3 concentration. This demonstrates that the structure is more open to the glassy system, which coincides with the higher NBOs in the FTIR measurements.

In context, the dielectric constant of BSCZG glasses increased from 2.32 to 2.48 with increasing Ga ions content in the glass matrix from 0 to 20 mol%. As shown in Table 3, a decrease in the optical bandgap results from the increase in the optical dielectric constant. The optical band gap and refractive index results indicate that gallium ions in these samples are optimal materials for optoelectronic applications.

3.5 After simulated body fluid SBF

XRD patterns of BSCZG glass samples, after immersion in simulated body fluid (SBF) for 3, 7, and 14 days, are depicted in Fig. 7a–c, respectively. The analysis of these XRD patterns reveals the emergence of hydroxyapatite (HA). Notably, the distinct HA peak is not observed in the BSCZG samples, except for BSCZG15 and BSCZG20. The observed linewidth peak at 2θ of 26° aligns with Card No. 98-008-2291 of the Inorganic Crystal Structure Database (ICSD). This observation is consistent with findings reported in numerous literature sources (Zhou et al. 2021; Sadeq and Ibrahim 2021).

On the other hand, the FTIR results confirmed hydroxyapatite (HA) formation in the BSCZG samples following immersion in simulated body fluid (SBF), as illustrated in Fig. 8. A noticeable change in the crystallization rate is observed between BSCZG15 and BSCZG20 as increasing the immersion time. This phenomenon can be attributed to the stepwise process of hydroxyapatite formation, involving ion exchange and material rearrangement, aligning with previously published findings (Woo et al. 2007). The

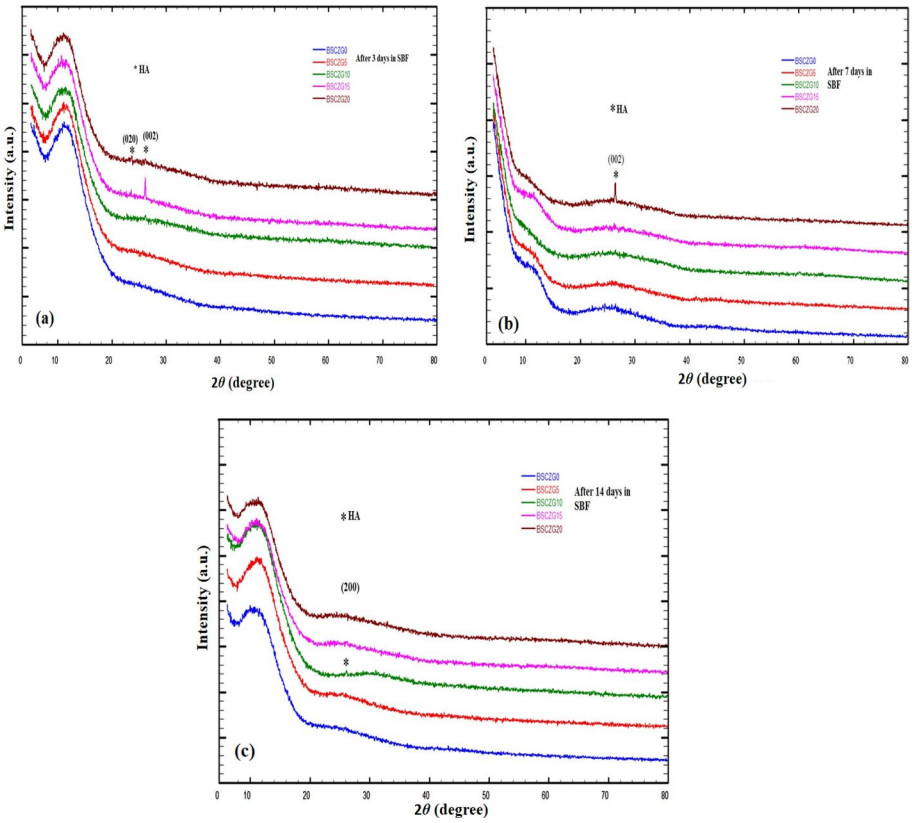

Fig. 7 XRD patterns of BSCZG samples after immersion in SBF **a** 3 days, **b** 7 days, and **c** 14 days

samples were immersed in SBF solution, maintained at approximately 37 °C, for durations ranging from 1 to 14 days. With increasing immersion time, new peaks emerged in the FTIR spectra within the 550–610 cm^{-1} range, as depicted in Fig. 8a–c.

Specifically, two bands at 570 cm^{-1} and 610 cm^{-1} (corresponding to P-O bands) signify the antisymmetric vibration mode of P-O in amorphous calcium phosphate, indicating HA formation after immersion in SBF (Sayyed et al. 2022; Sadeq and Ibrahim 2021; Farag et al. 2022). Around 560 cm^{-1}, a single peak or a split peak became evident for these samples. The presence of crystalline calcium phosphates, including hydroxyapatite (HA), is signaled by this region, which is particularly distinctive for apatite and other phosphates. It corresponds to P-O bonding vibrations within a PO_3^{4-} tetrahedron. According to Videau and Dupuis, a single peak in this region indicates the formation of non-apatite or amorphous calcium phosphate (ACP), typically considered a precursor to hydroxyapatite (Sayyed et al. 2022; Sadeq and Ibrahim 2021). As Jones, Sepulveda, and Hench described, apatite PO_3^{4-} groups exhibit distinct split bands at 530 and 610 cm^{-1} (Farouk et al. 2020). It is plausible that BSCZG glasses with higher concentrations of Ga_2O_3 may contain more apatite and other phosphates, thereby increasing the network's apatite content.

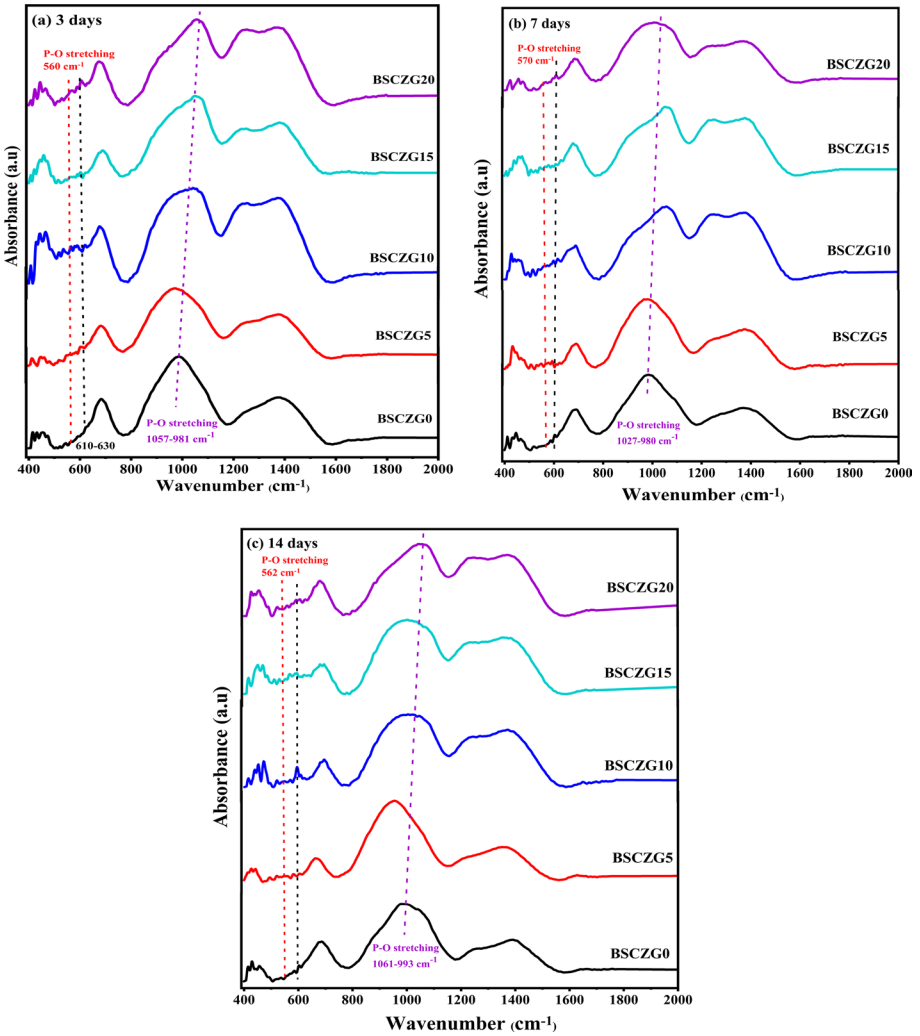

Fig. 8 FTIR spectra of BSCZG glasses with '*x*' of 0, 5, 10, 15, and 20 mol.% Ga_2O_3 content after immersion SBF **a** 3 days, **b** 7 days, and **c** 14 days

3.6 Proteins adsorption

The behavior of protein adsorption is significantly influenced by biomaterials' chemical composition and surface charge (Woo et al. 2007). This influence arises from reactions between functional groups present on proteins and those on the surfaces of glass samples. To assess the adsorption behavior of the produced samples, they were immersed for 1 h at 37 °C in a plastic beaker containing a 10 mg mL^{-1} solution of bovine serum albumin (BSA) dissolved in phosphate-buffered saline (PBS). Figure 9 and Table 4 illustrate the disintegration of the amide I and amide II bands in the spectrum due to BSA adsorption at the interfaces of the samples. Specifically, in the BSCZG0 sample, the amide I band

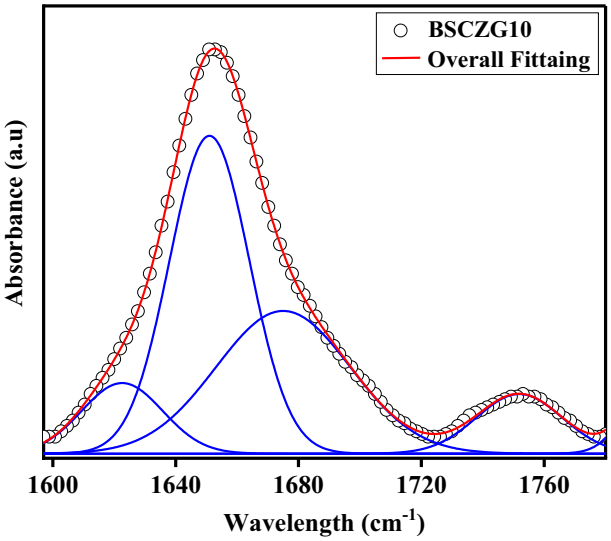

Fig. 9 Deconvoluted IR spectra of Amide I and Amide II bands of BSA adsorbed on BSCZG10-glass

Table 4 Deconvoluted IR spectra in the range (1600–1780 cm^{-1}) of Amide I and Amide II bands of BSA adsorbed of BSCZG-glasses

No. peak	Band center (cm^{-1})				
	BSCZG0	BSCZG5	BSCZG10	BSCZG15	BSCZG20
1	1621	1629	1622	1618	1619
2	1645	1653	1651	1648	1649
3	1673	1680	1675	1681	1682
4	1738	1747	1751	1742	1743

initially appears at 1738 cm^{-1}, while in BSCZG20, this peak shifts to a higher wavenumber that is observed at 1743 cm^{-1} (Bouhekka and Bürgi 2012). Additionally, the amide II band at 1673 cm^{-1} in the BSCZG0 sample shifts to 1645 cm^{-1} (III) and 1621 cm^{-1} (IV) in BSCZG0.

In contrast, in BSCZG20-glass, the center of this peak shifts to a lower wavenumber, specifically at 1619 cm^{-1}. The ratio of Amide I to Amide II on all sample surfaces increased with higher concentrations of Ga ions in the borosilicate glass matrix. This observation aligns with the widely accepted hypothesis that electromagnetic interactions are crucial in protein adsorption (Healy and Ducheyne 1992). Furthermore, the results of FTIR analysis after protein adsorption (as shown in Fig. 9 and Table 4) indicate the increase in hydroxyl groups (OH^-) with the increase of Ga_2O_3 content. This, in turn, leads to enhanced interactions between Ga^{3+} ions and the prepared bio-glasses, resulting in more significant protein adsorption due to the interaction between the NH_2 amino group of BSA and the OH^-. Additionally, the FTIR data (as seen in Fig. 3 and Table 1) reveal an increase in non-bridging oxygen (NBOs) groups in the (BO_3) range, suggesting that more addition of Ga_2O_3 produces more NBOs groups. This may indicate a tendency for the network structure of the prepared glasses to adopt more open configuration, which improves protein absorption (Healy and Ducheyne 1992).

3.7 Cell viability

MTT analyses were conducted on Vero cell lines to evaluate the cytotoxicity of the compounds, with varying concentrations of each compound. As depicted in Fig. 10a–e, following 48 h of incubation, the relative cell viability exhibited a range of responses, spanning from BSCZG5μg.ml^{-1} to BSCZG20 μg.ml^{-1}.

Figure 10 demonstrates that the half-maximal inhibitory concentration (IC50) values nearly double, increasing from 11.27 to 23.84 μg ml^{-1} as the Ga_2O_3 content varies from 0 to 20 mol%. These IC50 results indicate the impact of gallium ions concentration

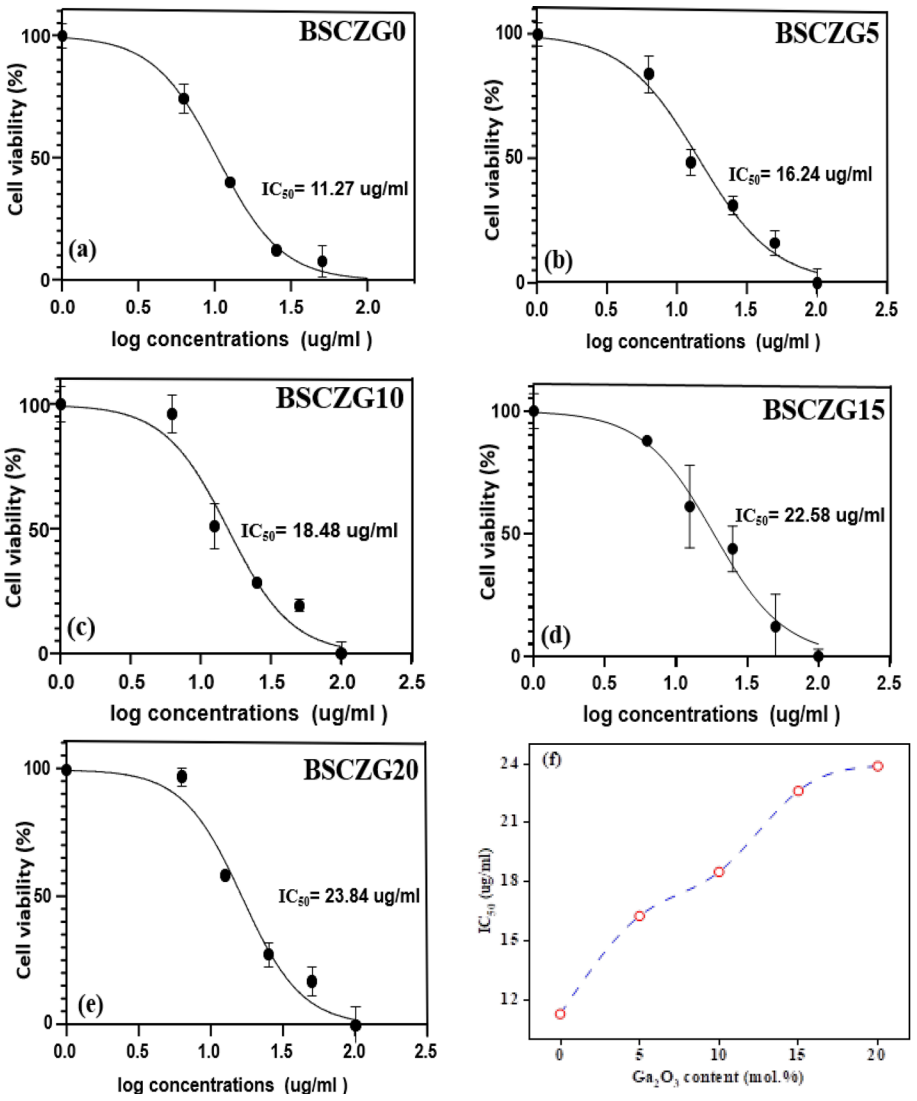

Fig. 10 The cell viability for BSCZG-glasses, **a** BSCZG0, **b** BSCZG5, **c** BSCZG10, **d** BSCZG15, **e** BSCZG20 and **f** the half- maximal inhibitory (IC_{50}) with increasing Ga_2O_3 content

in borosilicate glass on cell growth. Bioactive glasses release ions into the surrounding fluid, promoting biocompatibility by releasing ions such as Si^{4+} and Ca^{2+}. This phenomenon has been established in previous studies (Zeimaran et al. 2016; Alcaide et al. 2010). Consequently, Ga-containing bioactive glass, which elicits cellular responses and enhances surface roughness, can achieve favorable cytocompatibility by releasing ions and surface modifications (Pourshahrestani et al. 2017).

Based on the results above, it can be inferred that the increase of gallium ions concentration leads to enhanced cellular compatibility.

4 Conclusion

Using the melt quenching technique, we prepared a novel bioactive glass system consisting of gallium calcium zinc borosilicate glasses. Comprehensive studies were conducted to investigate the prepared samples' structure, physical, optical, and biomedical properties. XRD analysis confirmed the amorphous nature of the as-prepared samples, and hydroxyapatite (HA) was verified after immersion in simulated body fluid (SBF) are observed from FTIR results. The addition of Ga_2O_3 from 0 to 20 mol% increased the formation of non-bridging oxygens (NBOs), as indicated by the FTIR data. Furthermore, with the increase of Ga_2O_3 content both molar volume and experimental density values increased, ranging from 24.66 to 29.58 cm^3 mol^{-1} and 2.70 to 3.14 g cm^{-3}, respectively. The optical band gap values decreased from 3.27 to 3.08 eV, while the optical band tail increased from 0.20 to 0.25 eV with increasing Ga_2O_3 content. These characteristics possies BSCZG glasses as optimal for optoelectronic applications. Interestingly, although the incorporation of Ga ions increased the number of NBOs in the glass matrix, it reduced the ability to transfer negative charges from the glass network to probe ions in the prepared glasses. Electronic polarizability, resulting from these materials, can enhance cell viability, as demonstrated by the sample with the highest Ga ions content exhibiting a higher rate of protein uptake compared to sample free of Ga ions. This electronic polarizability enables electronic and optical applications and enhances the samples capability to absorb proteins. Finally, our findings indicate that these novel Ga free, Ga-borosilicate glasses are promising for biomedical applications due to their favorable characteristics. However, further investigation into Ga-borosilicate activity in vivo is imperative for clinical utilization.

Acknowledgements Not Applicable

Author contributions All authors contributed to the study's conception and design. Materials preparation was performed by TMT, AI, and MYH. Data collection and analysis were performed by all; further, AFM accomplished the structure analysis. The original draft of the manuscript was written by AI, and then all authors contributed to the discussion and revised the manuscript. All authors read and approved the final manuscript.

Funding Not applicable.

Data availability The datasets used and/or analyzed during the current study are available from the corresponding author on reasonable request. Contact corresponding author: elawadyahmed59@gmail.com.

Declarations

Conflict of interest The authors declare that they have no known competing financial interests or personal relationships that could have appeared to influence the work reported in this paper.

Ethics approval Not Applicable.

References

Abd El-Fattah, Z.M., Ahmad, F., Hassan, M.A.: Tuning the structural and optical properties in cobalt oxide-doped borosilicate glasses. J. Alloys Compd. **728**, 773–779 (2017). https://doi.org/10.1016/j.jallcom.2017.09.059

Alcaide, M., Portolés, P., López-Noriega, A., et al.: Interaction of an ordered mesoporous bioactive glass with osteoblasts, fibroblasts and lymphocytes, demonstrating its biocompatibility as a potential bone graft material. Acta Biomater. **6**, 892–899 (2010). https://doi.org/10.1016/j.actbio.2009.09.008

Al-Hadeethi, Y., Sayyed, M.I., Kaewkhao, J., et al.: An extensive investigation of physical, optical and radiation shielding properties for borate glasses modified with gadolinium oxide. Appl. Phys. A **125**, 749, 1-10 (2019). https://doi.org/10.1007/s00339-019-3053-3

Bai, N., Chen, W., Luo, L., et al.: Effect of B_2O_3 on the structural and in vitro biological assessment of mesoporous bioactive glass nanospheres. J. Am. Ceram. Soc. **104**, 3058–3072 (2021). https://doi.org/10.1111/jace.17653

Ballato, J., Dragic, P.D.: Glass: the carrier of light—Part II—A brief look into the future of optical fiber. Int. J. Appl. Glass Sci. **12**, 3–24 (2021). https://doi.org/10.1111/ijag.15844

Blanc, W., Choi, Y.G., Zhang, X., Nalin, M., Richardson, K.A., Righini, G.C., Ferrari, M., Jha, A., Massera, J., Jiang, S., Ballato, J., Petit, L.: The past, present and future of photonic glasses: a review in homage to the United Nations international year of glass 2022. Prog. Mater. Sci. **134**, 101084 (2023). https://doi.org/10.1016/j.pmatsci.2023.101084

Bouhekka, A., Bürgi, T.: Photodegradation of adsorbed bovine serum albumin on TiO_2 anatase investigated by in-situ ATR-IR spectroscopy. Acta Chim. Slov. **59**, 841–847 (2012)

Boyjoo, Y., Wang, M., Pareek, V.K., Liu, J., Jaronie, M.: Synthesis and applications of porous non-silica metal oxide submicrospheres. Chem. Soc. Rev. **45**, 6013 (2016). https://doi.org/10.1039/c6cs00060f

Brink, M., Turunen, T., Happonen, R.-P., Yli-Urpo, A.: Compositional dependence of bioactivity of glasses in the system Na_2O–K_2O–MgO–CaO–B_2O_3–P_2O_5–SiO_2. J. Biomed. Mater. Res. **37**, 114–121 (1997). https://doi.org/10.1002/(SICI)1097-4636(199710)37:1%3c114:AID-JBM14%3e3.0.CO;2-G

Catauro, M., Bollino, F., Renella, R.A., Papale, F.: Sol–gel synthesis of SiO_2–CaO–P_2O_5 glasses: influence of the heat treatment on their bioactivity and biocompatibility. Ceram. Int. **41**, 12578–12588 (2015). https://doi.org/10.1016/J.CERAMINT.2015.06.075

Chen, R., Li, Q., Zhang, Q., et al.: Nanosized HCA-coated borate bioactive glass with improved wound healing effects on rodent model. Chem. Eng. J. **426**, 130299 (2021). https://doi.org/10.1016/j.cej.2021.130299

Collery, P., Keppler, B., Madoulet, C., Desoize, B.: Gallium in cancer treatment. Crit. Rev. Oncol. Hematol. **42**, 283–296 (2002). https://doi.org/10.1016/S1040-8428(01)00225-6

De Assis, A.S.J., Pegoraro, G.M., Duarte, I.C.S.: Evolution of gallium applications in medicine and microbiology: A timeline. Biometals **35**, 675–688 (2022). https://doi.org/10.1007/s10534-022-00406-4

Deliormanlı, A.M.: Synthesis and characterization of cerium- and gallium-containing borate bioactive glass scaffolds for bone tissue engineering. J. Mater. Sci. Mater. Med. **26**, 67 (2015). https://doi.org/10.1007/s10856-014-5368-0

Doadrio, A.L., Sánchez-Montero, J.M., Doadrio, J.C., et al.: Mesoporous silica nanoparticles as a new carrier methodology in the controlled release of the active components in a polypill. Eur. J. Pharm. Sci. **97**, 1–8 (2017). https://doi.org/10.1016/j.ejps.2016.11.002

El-Daly, A.A., Abdo, M.A., Bakr, H.A., Sadeq, M.S.: Impact of cobalt ions on the phonon energy and ligand field parameters of some borate glasses. J. Non Cryst. Solids **555**, 120535 (2021). https://doi.org/10.1016/j.jnoncrysol.2020.120535

Farag, M.A., Ibrahim, A., Hassaan, M.Y., Ramadan, R.M.: Enhancement of structural and optical properties of transparent sodium zinc phosphate glass–ceramics nano composite. J. Aust. Ceram. Soc. **58**, 653–661 (2022). https://doi.org/10.1007/s41779-022-00716-3

Farouk, M., Samir, A., Ibrahim, A., et al.: Raman, FTIR studies and optical absorption of zinc borate glasses containing WO_3. Appl. Phys. A **126**, 696 (2020). https://doi.org/10.1007/s00339-020-03890-y

Franchini, M., Lusvardi, G., Malavasi, G., Menabue, L.: Gallium-containing phospho-silicate glasses: Synthesis and in vitro bioactivity. Mater. Sci. Eng. C **32**, 1401–1406 (2012). https://doi.org/10.1016/j.msec.2012.04.016

Healy, K.E., Ducheyne, P.: Hydration and preferential molecular adsorption on titanium in vitro. Biomaterials **13**, 553–561 (1992). https://doi.org/10.1016/0142-9612(92)90108-Z

Hench, L.L., Roki, N., Fenn, M.B.: Bioactive glasses: importance of structure and properties in bone regeneration. J. Mol. Struct. **1073**, 24–30 (2014). https://doi.org/10.1016/j.molstruc.2014.03.066

Ibrahim, A., Sadeq, M.S.: Influence of cobalt oxide on the structure, optical transitions and ligand field parameters of lithium phosphate glasses. Ceram. Int. **47**, 28536–28542 (2021). https://doi.org/10.1016/j.ceramint.2021.07.011

Ibrahim, A., Farag, M.A., Sadeq, M.S.: Towards highly transparent tungsten zinc sodium borate glasses for radiation shielding purposes. Ceram. Int. **48**, 12079–12090 (2022). https://doi.org/10.1016/j.ceramint.2022.01.068

Ibrahim, A., Kubo, K., Watanabe, S., Shiba, S., Khan, I., Zhang, B., Homonnay, Z., Kuzmann, E., Pavić, L., Santić, A., Ali, A.S., Hassaan, M.Y., Kubuki, S.: Enhancement of electrical conductivity and thermal stability of iron- or tin- substituted vanadate glass and glass-ceramics nanocomposite to be applied as a high-performance cathode active material in sodium-ion batteries. J. Alloys Compd. **930**, 167366 (2023a). https://doi.org/10.1016/j.jallcom.2022.167366

Ibrahim, A., Arita, Y., Ali, A.S., Khan, I., Zhang, B., Razum, M., Pavić, L., Santić, A., Homonnay, Z., Kuzmann, E., Hassaan, M.Y., Wang, J., Kubuki, S.: Impact of adding Fe ions on the local structure and electrochemical performance of P_2O_5–V_2O_5 glass and glass ceramics used as a cathode in LIBs. J. Phys. Chem. Solids **179**, 111391 (2023b). https://doi.org/10.1016/j.jpcs.2023.111391

Ibrahim, A., Shiraishi, M., Homonnay, Z., Krehula, S., Marciuš, M., Bafti, A., Pavic, L., Kubuki, S.: Photocatalytic and cathode active abilities of Ni-substituted α-FeOOH nanoparticles. Int. J. Mol. Sci. **24**, 14300 (2023c). https://doi.org/10.3390/ijms241814300

Jones, J.R.: Review of bioactive glass: from Hench to hybrids. Acta Biomater. **9**, 4457–4486 (2013). https://doi.org/10.1016/j.actbio.2012.08.023

Kamal, H., Hezma, A.M.: Structure and physical properties of borosilicate as potential bioactive glasses. SILICON **10**, 851–858 (2018). https://doi.org/10.1007/s12633-016-9540-7

Lai, Y., Zeng, Y., Tang, X., Zhang, H., Hanb, J., Su, H.: Structural investigation of calcium borosilicate glasses with varying Si/ca ratios by infrared and raman spectroscopy. RSC Adv. **6**, 93722 (2016). https://doi.org/10.1039/C6RA20969F

Mabied, A.F., Shalaby, A.R., Ramadan, A.A., et al.: Study on quality of pair distribution function for direct space approach of structure investigation. Int. J. Thin Film Sci. Technol. (2022). https://doi.org/10.18576/ijtfst/110118

Mansour, S.F., Wageh, S., Alotaibi, M.F., Abdo, M.A., Sadeq, M.S.: Impact of bismuth oxide on the structure, optical features and ligand field parameters of borosilicate glasses doped with nickel oxide. Ceram. Int. **47**, 21443–21449 (2021). https://doi.org/10.1016/j.ceramint.2021.04.154

Ojansivu, M., Mishra, A., Vanhatupa, S., et al.: The effect of S53P4-based borosilicate glasses and glass dissolution products on the osteogenic commitment of human adipose stem cells. PLoS ONE **13**, 0202740 (2018). https://doi.org/10.1371/journal.pone.0202740

Pourshahrestani, S., Zeimaran, E., Kadri, N.A., et al.: Potency and cytotoxicity of a novel gallium-containing mesoporous bioactive glass/chitosan composite scaffold as hemostatic agents. ACS Appl. Mater. Interfaces **9**, 31381–31392 (2017). https://doi.org/10.1021/acsami.7b07769

Quintero Sierra, L.A., Escobar, D.M.: Characterization and bioactivity behavior of sol-gel derived bioactive vitroceramic from non-conventional precursors. Bol. Soc. Esp. Ceram. Vidrio **58**, 85–92 (2019). https://doi.org/10.1016/j.bsecv.2018.07.003

Rana, K., Souza, L.P., Isaacs, M.A., Raja, F., Morrell, A.P., Martin, R.A.: The development and characterisation of gallium doped bioactive glasses for potential bone cancer applications. ACS Biomater. Sci. Eng. **3**(12), 3425–3432 (2017). https://doi.org/10.1021/acsbiomaterials.7b00283

Ren, M., Lu, X., Deng, L., et al.: B_2O_3/SiO_2 substitution effect on structure and properties of Na_2O–CaO–SrO–P_2O_5–SiO_2 bioactive glasses from molecular dynamics simulations. Phys. Chem. Chem. Phys. **20**, 14090–14104 (2018). https://doi.org/10.1039/C7CP08358K

Sadeq, M.S., Ibrahim, A.: The path towards wide-bandgap and UV-transparent lithium phosphate glasses doped with cobalt oxide for optical applications. J. Non Cryst. Solids **569**, 120983 (2021). https://doi.org/10.1016/j.jnoncrysol.2021.120983

Sayyed, M.I., Issa, S.A., Tekin, H.O., Saddeek, Y.B.: Comparative study of gamma-ray shielding and elastic properties of BaO–Bi_2O_3–B_2O_3 and ZnO–Bi_2O_3–B_2O_3 glass systems, Matter. Chem. Phys. **217**, 11–22 (2018). https://doi.org/10.1016/j.matchemphys.2018.06.034

Sayyed, M.I., Ibrahim, A., Abdo, M.A., Sadeq, M.S.: The combination of high optical transparency and radiation shielding effectiveness of zinc sodium borate glasses by tungsten oxide additions. J. Alloys Compd. **904**, 164037 (2022). https://doi.org/10.1016/j.jallcom.2022.164037

Sistla, R.K., Seshasayee, M.: Structural study of lithium phosphate glasses by X-ray RDF and computer simulations. J. Non Cryst. Solids **349**, 22–29 (2004). https://doi.org/10.1016/j.jnoncrysol.2004.08.257

Tiama, T.M., Ibrahim, M.A., Sharaf, M.H., Mabied, A.F.: Effect of germanium oxide on the structural aspects and bioactivity of bioactive silicate glass. Sci. Rep. **13**, 9582 (2023). https://doi.org/10.1038/s41598-023-36649-5

Tostanoski, N.J., Möncke, D., Youngman, R., Sundaram, S.K.: Structure-terahertz property relationship in sodium borosilicate glasses. Int. J. Appl. Glass Sci. (2022). https://doi.org/10.1111/ijag.16608
Tripathi, H., Singh, S.P., Arepalli, S.K., et al.: Studies on preparation and characterization of 45S5 bioactive glass doped with (TiO_2+ZrO_2) as bioactive ceramic material. Bioceram. Dev. Appl. **06**, 2090–5025 (2016). https://doi.org/10.4172/2090-5025.1000090
Valappil, S.P., Ready, D., Abou Neel, E.A., et al.: Controlled delivery of antimicrobial gallium ions from phosphate-based glasses. Acta Biomater. **5**, 1198–1210 (2009). https://doi.org/10.1016/j.actbio.2008.09.019
Vallet-Regi, M., Rámila, A., del Real, R.P., Pérez-Pariente, J.: A new property of MCM-41: drug delivery system. Chem. Mater. **13**, 308–311 (2001). https://doi.org/10.1021/cm0011559
Vallet-Regí, M., Colilla, M., Izquierdo-Barba, I., Manzano, M.: Mesoporous silica nanoparticles for drug delivery: current insights. Molecules **23**, 47 (2017). https://doi.org/10.3390/molecules23010047
Vukajlovic, D., Novakovic, K., Bretcanu, O.: Self-crystallisation, an unexpected property of 45S5 Bioglass®. Chem. Commun. **57**, 13558–13561 (2021). https://doi.org/10.1039/D1CC04847C
Woo, K.M., Seo, J., Zhang, R., Ma, P.X.: Suppression of apoptosis by enhanced protein adsorption on polymer/hydroxyapatite composite scaffolds. Biomaterials **28**, 2622–2630 (2007). https://doi.org/10.1016/j.biomaterials.2007.02.004
Wren, A.W., Keenan, T., Coughlan, A., et al.: Characterisation of Ga_2O_3–Na_2O–CaO–ZnO–SiO_2 bioactive glasses. J. Mater. Sci. **48**, 3999–4007 (2013). https://doi.org/10.1007/s10853-013-7211-2
Zeimaran, E., Mohan, S., Pourshahrestani, S., et al.: Osteogenic differentiation of mesenchymal stem cells on a poly (octanediol citrate)/bioglass composite scaffold in vitro. Mater. Des. **109**, 434–442 (2016). https://doi.org/10.1016/j.matdes.2016.07.096
Zheng, K., Boccaccini, A.R.: Sol-gel processing of bioactive glass nanoparticles: a review. Adv. Colloid Interface Sci. **249**, 363–373 (2017). https://doi.org/10.1016/j.cis.2017.03.008
Zhou, J., Liao, Q., Wang, F., et al.: Effect of Na_2O and CaO on the solubility and crystallization of Mo in borosilicate glasses. J. Non-Cryst. Solids **557**, 120623 (2021). https://doi.org/10.1016/j.jnoncrysol.2020.120623
Zhu, H., Zheng, K., Boccaccini, A.R.: Multi-functional silica-based mesoporous materials for simultaneous delivery of biologically active ions and therapeutic biomolecules. Acta Biomater. **129**, 1–17 (2021). https://doi.org/10.1016/j.actbio.2021.05.007

Authors and Affiliations

Taha M. Tiama[1] · A. Ibrahim[2,3] · M. Y. Hassaan[3] · Ahmed F. Mabied[4]

✉ A. Ibrahim
elawadyahmed59@gmail.com

✉ M. Y. Hassaan
myhassaan@yahoo.com

[1] Department of Basic Sciences, October High Institute of Engineering and Technology - OHI, 6th of October City, Giza, Egypt

[2] Basic Sciences Department, Faculty of Engineering, Sinai University, El Qantara, Egypt

[3] Department of Physics, Faculty of Science, Al-Azhar University, Nasr City, Cairo 11884, Egypt

[4] X-Ray Crystallography Laboratory, Solid State Physics Department, National Research Centre, Dokki, Giza 12622, Egypt